

Registration-free Distortion Correction of Diffusion Weighted MRI

Kurt G Schilling^{*1,2}, Justin Blaber^{*3}, Colin Hansen⁴, Baxter Rogers^{1,2}, Adam W Anderson^{1,2,4}, Seth Smith^{1,2,4}, Praitayini Kanakaraj³, Tonia Rex⁶, Susan M. Resnick⁷, Andrea T. Shafer⁷, Laurie Cutting⁸, Neil Woodward⁹, David Zald¹⁰, Bennett A Landman^{1,2,3}

¹Radiology and Radiological Sciences, Vanderbilt University Medical Center, Nashville, TN

²Vanderbilt University Institute of Imaging Science, Vanderbilt University, Nashville, TN

³Electrical Engineering, Vanderbilt University, Nashville, TN

⁴Computer Science, Vanderbilt University, Nashville, TN

⁵Biomedical Engineering, Vanderbilt University, Nashville, TN

⁶Vanderbilt Eye Institute, Vanderbilt University Medical Center, Nashville, TN

⁷Laboratory of Behavioral Neuroscience, National Institute on Aging, National Institutes of Health, Baltimore, MD, United States of America

⁸Special Education, Vanderbilt University, Nashville, TN

⁹Psychiatry and Behavioral Sciences, Vanderbilt University Medical Center, Nashville, TN

¹⁰Neuroscience, Vanderbilt University, Nashville, TN

*authors contributed equally to this work

Correspondence: kurt.g.schilling.1@vumc.org

, address, phone

Abstract

Diffusion magnetic resonance images may suffer from geometric distortions due to susceptibility induced off resonance fields, which cause geometric mismatch with anatomical images and ultimately affect subsequent quantification of microstructural or connectivity indices. State-of-the-art diffusion distortion correction methods typically require data acquired with reverse phase encoding directions, resulting in varying magnitudes and orientations of distortion, which allow estimation of an undistorted volume. Alternatively, additional field maps acquisitions can be used along with sequence information to determine warping fields. However, not all imaging protocols include these additional scans and cannot take advantage of state-of-the-art distortion correction. To avoid additional acquisitions, structural MRI (undistorted scans) can be used as registration targets for intensity driven correction. In this study, we aim to (1) enable susceptibility distortion correction with historical and/or limited diffusion datasets that do not include specific sequences for distortion correction and (2) avoid the computationally intensive registration procedure typically required for distortion correction using structural scans. To achieve these aims, we use deep learning (3D U-nets) to synthesize an undistorted b0 image that matches geometry of structural T1w images and intensity contrasts from diffusion images. Importantly, the training dataset is heterogenous, consisting of varying acquisitions of both structural and diffusion. We apply our approach to a withheld test set and show that distortions are successfully corrected after processing. We quantitatively evaluate the proposed distortion correction and intensity-based registration against state-of-the-art distortion correction (FSL topup). The results illustrate that the proposed pipeline results in b0 images that are geometrically similar to non-distorted structural images, and more closely match state-of-the-art correction with additional acquisitions. In addition, we show generalizability of the proposed approach to datasets that were not in the original training / validation / testing datasets. These datasets included varying populations, contrasts, resolutions, and magnitudes and orientations of distortion and show efficacious distortion correction. The method is available as a Singularity container, source code, and an executable trained model to facilitate evaluation.

Keywords: Diffusion, Magnetic Resonance Imaging, Brain, Distortion Correction, Deep Learning

1. Introduction

The rapid echo planar imaging techniques and high gradient fields typically used for diffusion weighted magnetic resonance imaging (DW-MRI) introduce geometric distortions in the reconstructed images. Initially, both the static field distortions (e.g., interactions of fast imaging techniques with inhomogeneities) and the gradient dependent effects (e.g., gradient field disturbances given eddy current effects) were corrected along with motion through registration^{1,2}. However, image-based approaches have two central problems. First, accurate inter-modality alignment between (distorted) DW-MRI imaging and (undistorted) T1w anatomical imaging is problematic, especially in areas with limited tissue contrast. Second, image registration does not

offer a mechanism for correcting signal pileup – areas of erroneous signal void and/or very bright signal. Modern approaches resolve these difficulties by acquiring additional information, either with a field map or supplementary diffusion acquisitions designed to be differently sensitive to susceptibility and eddy effects (so called “blip-up blip-down” designs). Field maps are effective, but offer limited robustness to acquisition artifacts³, and the blip-up/blip-down studies are widely used, including in the Human Connectome Project⁴.

Current tools such as FSL’s topup⁵ and TORTOISE⁶, use minimally weighted DW-MRI images acquired with different phase-encoding parameters to estimate the static susceptibility field maps. Then, a

subsequent pass uses the diffusion weighted images to model and correct for the eddy current effects (e.g., FSL's eddy⁷ and TORTOISE's DR-BUDDI⁸). Techniques and datasets for benchmarking^{9,10} and quality control¹¹ are actively being explored, as obtaining a sufficiently high quality ground truth that is generalizable to clinical studies is difficult. Moreover, there is active research on correction techniques for DW-MRI outside of the brain, e.g., prostate¹² and spinal cord¹³.

Despite the availability of effective tools, the supplementary information necessary for these techniques is not always available, which could be potentially due to scanner limitations, scan time constraints, acquisition difficulties / artifacts, or legacy considerations. Recently, we presented a deep learning synthesis approach, Synb0-DisCo, to estimate non-distorted (infinite bandwidth) minimally weighted images from T1 weighed (T1w) images¹⁴. Synb0-DisCo uses a 2.5D (multi-slice, multi-view) generative adversarial network (GAN) to perform the image synthesis process.

While Synb0-DisCo is a promising first approach for a deep learning solution to the DW-MRI distortion correction problem, it has several limitations. First, Synb0-DisCo does not intrinsically compensate for absolute intensities of the target minimally weighed scans, and therefore, secondary adjustment of the intensity spaces is needed. Second, patient specific contrasts seen in the acquired distorted DW-MRI cannot be learned as the network only had relatively homogeneous T1w MRI information available. Third, Synb0-DisCo is susceptible to 3D inconsistencies as the model did not have access to full imaging context.

Herein, we propose a second generation of our deep learning approach, termed Synb0, for DW-MRI distortion correction to address these limitations. Briefly, we generalize the learning approach to use both T1w and distorted DW-MRI images, redesign the network to use full 3-D information, and train across a much larger collection of patients / studies / scanners. We evaluate Synb0 using three unique datasets with varying image quality, contrast, and acquisitions with baseline consideration of image registration, Synb0-DisCo, and no correction relative to the best available techniques using supplementary acquisitions.

2. Materials and Methods

The high-level overall pipeline is shown in **Figure 1**. The aim is to synthesize an undistorted b_0 from an input distorted single blip b_0 and a T1 anatomical image. Using the topup setting of infinite bandwidth will correct for known deformations and movement to match the undistorted

image perfectly and provide the necessary estimations to proceed with eddy current correct (e.g., with FSL's eddy).

2.1 Data

The data used for this study were retrieved in de-identified form from the Baltimore Longitudinal Study of Aging (BLSA), Human Connectome Project (HCP), and Vanderbilt University. Importantly, these datasets have varying resolutions, signal-to-noise ratios, T1 and diffusion contrasts, magnitudes of distortions, and directions of distortions.

Briefly, BLSA acquisition included T1-weighted images acquired using an MPRAGE sequence (TE = 3.1 ms, TR = 6.8 ms, slice thickness = 1.2 mm, number of Slices = 170, flip angle = 8 deg, FOV = 256x240mm, acquisition matrix = 256x240, reconstruction matrix = 256x256, reconstructed voxel size = 1x1mm). Diffusion acquisition was acquired using a single-shot EPI sequence, and consisted of a single b-value ($b = 700 \text{ s/mm}^2$), with 33 volumes (1 $b_0 + 32$ DWIs) acquired axially (TE = 75 ms, TR = 6801 ms, slice thickness = 2.2 mm, number of slices = 65, flip angle = 90 degrees, FOV = 212*212, acquisition matrix = 96*95, reconstruction matrix = 256*256, reconstructed voxel size = 0.83). HCP acquisition included T1-weighted images acquired using a 3D MPRAGE sequence (TE = 2.1 ms, TR = 2400 ms, slice thickness = 0.7 mm, flip angle = 8 deg, FOV = 224x224mm, acquisition, voxel size = 0.7x0.7mm). Diffusion acquisition was acquired using a single-shot EPI sequence, and consisted of three b-values ($b = 1000, 2000, \text{ and } 3000 \text{ s/mm}^2$), with 90 directions (and 6 $b=0 \text{ s/mm}^2$) per shell (TE = 89.5 ms, TR = 5520 ms, slice thickness = 1.25 mm, flip angle = 78 degrees, FOV = 210*180, voxel size = 1.25mm isotropic). The scans collected at Vanderbilt were part of healthy controls from several projects a typical acquisition is below, although some variations exist across projects. T1-weighted images acquired using an MPRAGE sequence (TE = 2.9 ms, TR = 6.3 ms, slice thickness = 1 mm, flip angle = 8 deg, FOV = 256x240mm, acquisition matrix = 256x240, voxel size = 1x1x1mm). Diffusion acquisition was acquired using a single-shot EPI sequence, and consisted of a three b-values ($b = 1000, 2000, 3000 \text{ s/mm}^2$), with 107 volumes (11 $b_0 + 96$ DWIs per shell) acquired axially (TE = 101 ms, TR = 5891 ms, slice thickness = 1.7 mm, flip angle = 90 degrees, FOV = 220*220, acquisition matrix = 144*144, voxel size = 1.7mm isotropic). We again note that variations in acquisition parameters exist in this dataset (resolution up to 2.5mm isotropic).

The data for training the network consists of T1 and distorted b_0 image

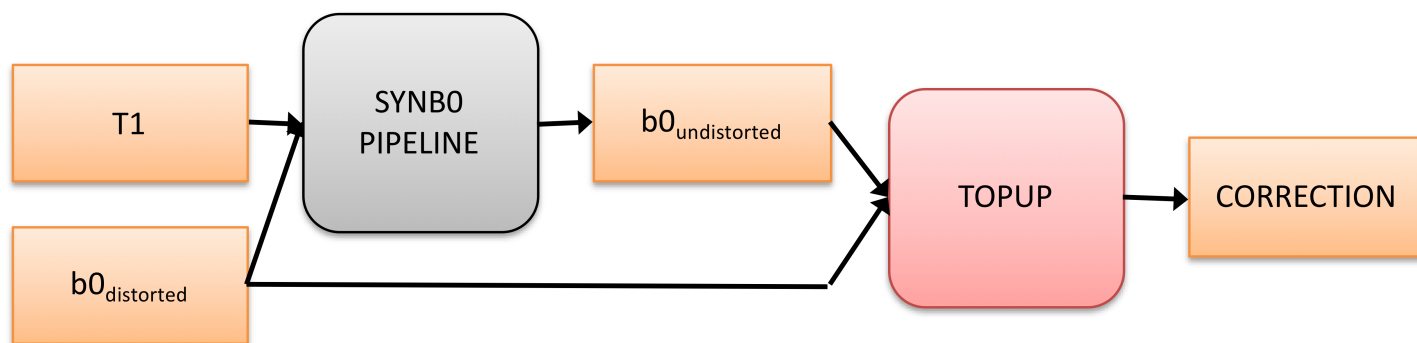


Fig. 1 Overall Pipeline. The goal is to generate an undistorted b_0 from a single blip (distorted) b_0 and an anatomical T1 image through a deep learning approach. The undistorted image can then be merged with the distorted b_0 and run through FSL's topup using a simulated infinite PE-bandwidth. This final correction can be used with FSL's eddy (or another eddy current modeling tool) to provide a full correction for diffusion data given only a single phase encoding. Note that the proposed algorithm does not seek to model/correct eddy current effects.

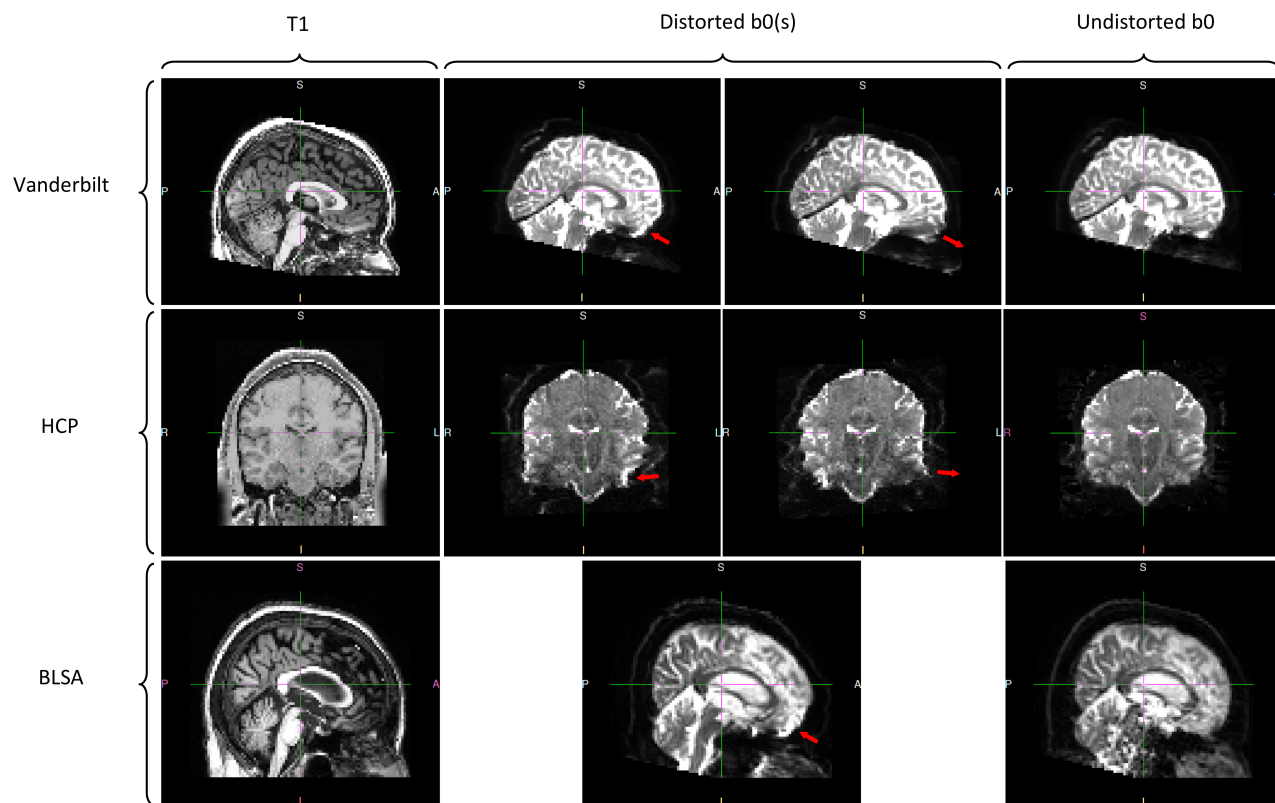


Fig. 2. Datasets used in this study. The b0's from Vanderbilt were acquired with opposite phase encodings along the A-P direction and corrected with topup. The b0s from HCP were acquired with opposite phase encodings along the L-R direction and corrected with topup. Lastly, b0s from BLSA were acquired with a single phase encoding along the A-P direction and corrected via a multi-shot EPI acquisition. The red arrows in the distorted b0 columns highlight areas of visible susceptibility distortion.

inputs and a truth of undistorted b0 images. For HCP and Vanderbilt, the undistorted b0 images were obtained by running topup on opposite phase encoded b0 images. For HCP, these phase encodings were L-R while for Vanderbilt, the phase encoding were A-P. For BLSA, the undistorted b0 images were obtained using a multi-shot EPI acquisition. The distorted b0 images from BLSA have a phase encoding along the A-P direction. Qualitative depictions of the data (T1, distorted, and undistorted processed b0's) are shown in **Figure 2**, while the number of datasets and scan information are shown in **Table 1**.

2.2 Preprocessing

The first step for preprocessing was a special step needed for the BLSA data because the intensities for the distorted b0 and undistorted b0 were slightly off due to the fact that the undistorted b0 was a separate acquisition. To account for this, the median value of the masked undistorted b0 was scaled such that it matched the masked median value of the undistorted b0. The rest of the data had undistorted b0s computed from topup, which have the same intensities as the distorted image. The rest of the preprocessing steps were applied to the rest of the data in the same manner.

A summary of the preprocessing is shown in **Figure 3**. The T1 image was intensity normalized using FreeSurfer's *mri_nu_correct*, *mni*, and *mri_normalize* which perform N3 bias field correction and intensity normalization, respectively on the input T1 image¹⁸. Next, the distorted b0 and undistorted b0 were coregistered to the skullstripped (via *bet*) T1 using FSL's *epi_reg*². The T1 was then affine registered using ANTS to a 1.0 mm isotropic MNI ICBM 152 asymmetric template¹⁹. The FSL

transform from *epi_reg* was converted to ANTS format using the *c3d_affine_tool* and the b0s were transformed into 2.5 mm isotropic MNI space via *antsApplyTransforms* and a resampled 2.5mm isotropic version of the MNI template. All transforms were saved so the inverse transform could be applied to bring the results back into subject space. Additionally, whole volume masks were created for the undistorted b0,

	Vanderbilt	HCP	BLSA
Subjects	38	488	424
Sessions	80	488	529
Phase Encoding	A-P	L-R	A-P
Correction	Topup	Topup	Multishot EPI
Resolution (mm)	1.7-2.5 iso	1.25mm iso	0.83x0.83x2.2
TE/TR	101/5891	89.5/5520	75/6801
Training splits (subjects)			
Learning (Training + Validation)	35	433	381
Testing (with-held)	3	55	43
External Validation			
	MASSIVE	Age-ility	Kirby21
Subjects	1	131	21
Sessions	18	131	42
Phase Encoding	A-P	I-P	A-P
Resolution (mm)	2.5 iso	2.2 iso	2.2 iso
TE/TR	100/7000	108/15,300	67/6281

Table 1. Data summary for Learning and Testing, and External Validation.

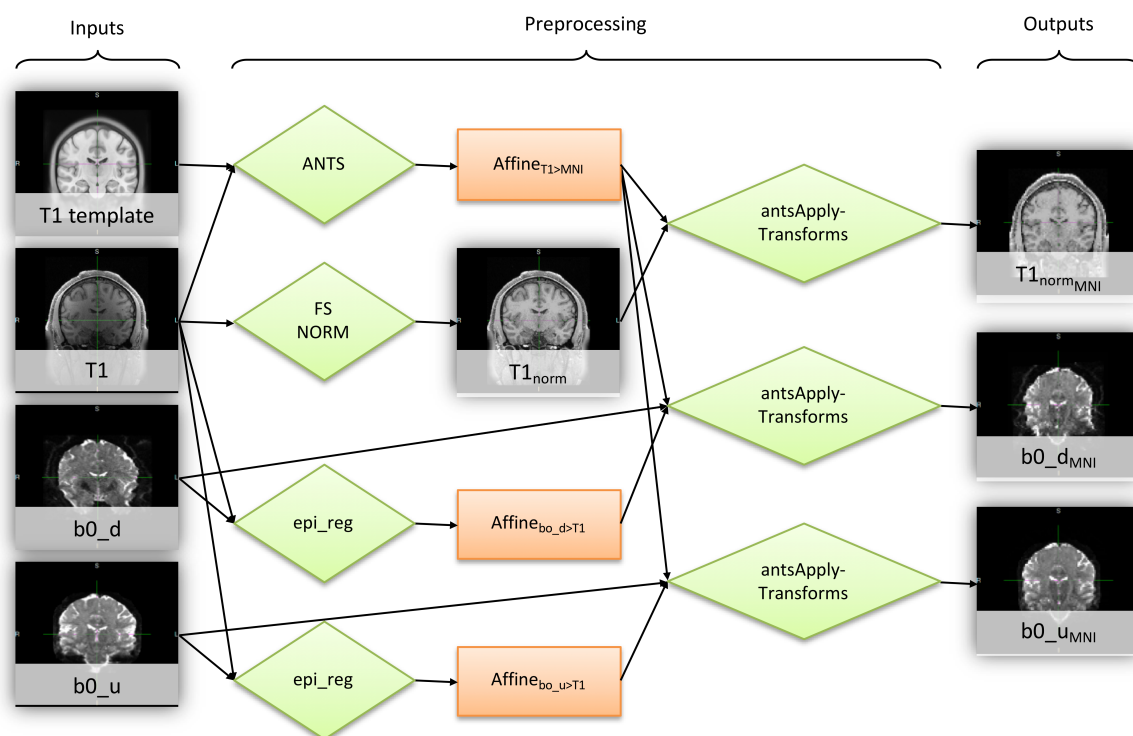


Fig. 3. The preprocessing pipeline. This figure shows data preparation prior to network learning (Fig. 4). The pipeline includes intensity normalization and alignment of the T1 image, the distorted b0, and undistorted b0 to T1 space. b0_d and b0_u represent the distorted and undistorted b0's, respectively.

distorted b0, and T1 and transforms were applied as needed to these masks to prevent training on regions where resampling could not be done.

Before training, the normalized 2.5 mm atlas aligned T1's intensities

were linearly scaled such that intensities ranging from 0 to 150 were mapped between -1 and 1. Fixed values of 0 and 150 could be used because of the FreeSurfer T1 intensity normalization as described. The distorted b0's intensities were scaled such that 0 to the 99th percentile were mapped between -1 and 1. Using the min and max of the distorted

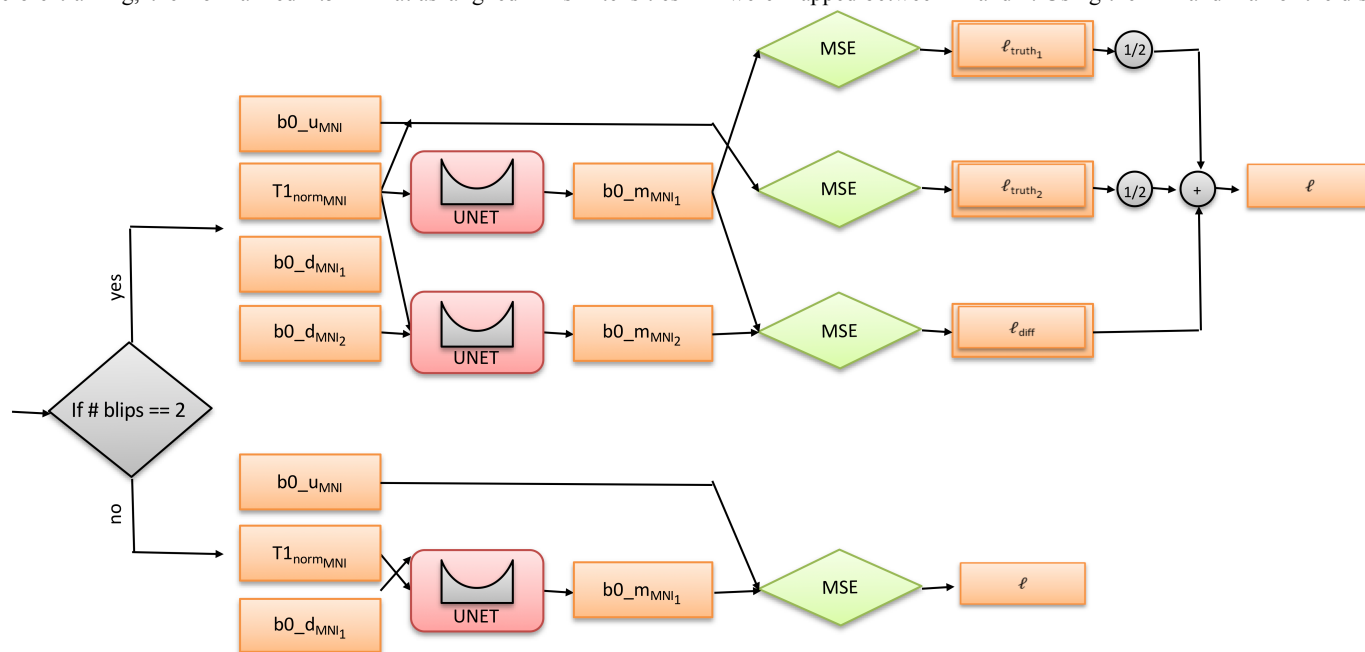


Fig. 4. Training Logic and loss calculation. For single blip b0's (BLSA; lower half of the decision tree), only the "truth" loss was computed. For two blip b0's (HCP and Vanderbilt; upper half of decision tree), two "truth" losses were computed, averaged, and then a "difference" loss term was added to obtain the final loss.

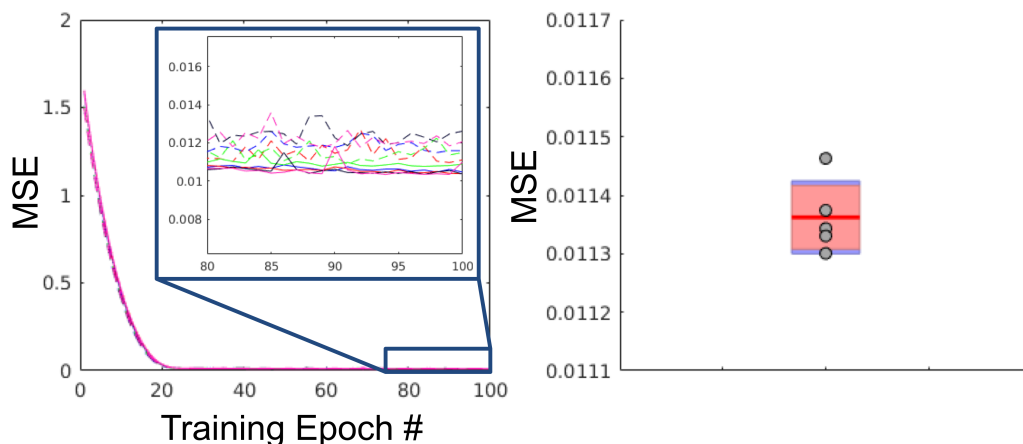


Fig. 5. Training, validation, and withheld loss. Left: Training and validation curves for each fold (5 training loss curves and 5 validation loss curves). The solid lines are the training curves and the dashed lines are the validation curves. Right: Plot of the MSE of the withheld test set (N=100) for each fold shown as green dots (5 folds) against a boxplot of the tail-end of the validation curves for each fold. Note that the test loss falls within the same range of the tail-end of the validation curves. here.

b0 was unstable due to signal pileup (which can cause localized large values). The 99th percentile was close enough to get the intensity of the cerebrospinal fluid mapped to 1. For the undistorted b0, the same 99th percentile value found for the undistorted image was used to scale it between -1 and 1. This was to ensure the same scaling was applied for the distorted and undistorted b0 since their overall intensities should be the same.

2.3 Network/Training/Loss

The network, inputs and outputs, and loss calculation are diagrammed in **Figure 4**. The network used to generate the undistorted b0 in 2.5 mm space was a 3D U-Net^{20,21} (2 channel input and 1 channel output), based on the original implementation in PyTorch²². Some differences were that leaky ReLU were used in place of ReLU. In addition, instance norm was used in place of batch norm since a small batch size was used. The implementation is available within a singularity container release (<https://www.singularity-hub.org/collections/3102>).

For training purposes, the data (organized in BIDS format²³) was partitioned across subjects for the test/validation/training sets. The data set was first partitioned into a test set of 100 random subjects and a “learning” set of 850 subjects. The test set was completely withheld. The “learning” set was again partitioned using 5-fold cross validation into training and validation sets (i.e., randomly shuffled into 680 testing and 170 validation for each fold).

The network trained for 100 epochs with a learning rate of 0.0001. Adam optimizer was used with betas set to 0.9 and 0.999. A weight decay of 1e-5 was applied. For each fold, the network was trained and after each epoch, the validation mean squared error (MSE) was computed and stored. The network with the lowest validation was selected for each fold as the most optimal network, resulting in 5 trained networks. Training was performed on Nvidia TITAN Xp GPUs with 12 GB of memory.

The loss function depended on the input data. For the BLSA subjects, since there was only single blip b0s, the output of the U-Net was compared directly to the undistorted image with MSE to generate the loss. For HCP and Vanderbilt images, there were two blip b0s. Both distorted b0s were passed through the network. Both outputs were compared with the undistorted b0 and the average of the two was stored

as the “truth” loss. In addition, the two outputs were compared via MSE loss and stored as the “difference” loss. These two losses were summed to get the final loss. The “truth” loss can be interpreted as minimizing the bias of the result (output should not deviate far from the truth). The “difference” loss can be interpreted as minimizing the variance of the result (outputs should be the same). For all losses computed, masks were used as described in the preprocessing section to only compute the loss in regions where resampling could be done. This strategy, of including both single blip data, as well as two-blip data, let’s the networks learn from distortions in a number of directions. This network architecture mirrors the Siamese²⁴ and null space²⁵ network designs.

2.4 Pipeline

For the final network, the five networks trained during cross validation were used and the ensemble average of the result was taken to get the synthesized undistorted b0 in affine MNI space. The inverse transforms were used to convert the generated undistorted b0 back into subject space. The distorted b0 was smoothed slightly to match the smoothness of the undistorted b0 because the output resolution of 2.5 mm isotropic from the network, followed by resampling back to subject space, resulting in some smoothing due to interpolation in the undistorted b0. We believe this is only required due to the fact that we are constrained to 2.5 mm isotropic for the network input due to GPU memory, so this step would be unnecessary if a higher resolution network on a GPU with more memory was used. The slightly smoothed distorted b0 and undistorted b0 were merged together and passed into topup with an acquisition parameters file containing two rows (see overall pipeline in **Figure 1**). The first row is a “dummy” row with arbitrary readout set, although care must be taken to ensure the arbitrary value is set in the correct column depending on the phase encoding direction. The second row is set with a readout of time of 0, which lets topup know that the second volume (the undistorted b0) contains no susceptibility distortion. The end result is the correction from topup which can be used as input into FSL’s eddy to perform a full diffusion imaging pre-processing which includes distortion, eddy current, and motion correction.

2.5 Quantitative Evaluation with Cross-Validation

To quantitatively investigate the geometric fidelity and contrasts of the images from the proposed pipeline, the resulting b0 images were compared to both the (undistorted) T1 image and the state-of-the art distortion correction (topup). For each of the classes of data (i.e.,

Vanderbilt, HCP, BLSA), 5 subjects were randomly selected from the withheld test set (i.e., had never been used in any part of the model selection process), resulting in 15 evaluations. For each, two measures were calculated. First, mutual information (MI) of the b0 with T1 was calculated as a measure of geometric similarity. Second, the mean-squared error of signal intensities between the synthesized correction and the topup correction is calculated, which assesses both distortion correction accuracy and contrast accuracy. For comparison, these measures were calculated with (A) the uncorrected b0, (B) a standard registration-based distortion correction method (that from Bhushan et al., 2012²⁶ implemented using the default parameters in BrainSuite software toolkit²⁷), and (C) the output from the proposed synthetic distortion correction (note that the synthesized b0 is not used for comparison, rather the acquired b0 after distortion correction is used for quantitative analysis).

2.6 Quantitative Evaluation with External Validation

We additionally chose three external validation datasets (not used in testing, training, nor validation steps) in order to validate our algorithm on data from sets entirely different from testing/training/validation. These include the “MASSIVE” brain dataset¹⁵, Kirby21 dataset¹⁶, and

the age-ility project dataset. Briefly the MASSIVE dataset¹⁵ was acquired on one subject over 18 sessions (T1 acquired at 1mm isotropic resolution using a 3D-TFE sequence, diffusion acquired at 2.5mm isotropic resolution, TE=100ms, TR=7000, flip angle=90, PE=AP direction), Kirby 21¹⁶ is a scan-rescan reproducibility dataset (T1 acquired at 1x1x1.2mm resolution using a MPRAGE sequence, diffusion acquired at 2.2mm isotropic resolution, TE=67ms, TR=6281, flip angle=90, PE=AP direction). Finally, Age-ility¹⁷ is a project that aims to investigate cognition and behavior across the lifespan, with phase 1 of the project including 131 subjects (T1 acquired at 1mm isotropic resolution using a MPRAGE sequence, diffusion acquired at 2mm isotropic resolution, TE=108ms, TR=15,300, flip angle=90, PE=AP direction).

3. Results

3.1 Results with Cross-Validation

The resulting training/validation and test results are shown in **Figure 5**. There are 5 validation curves (dashed lines) and 5 training curves (solid lines) since 5-fold cross validation was used. Note that the test MSE falls within the same range of the tail end of the training/validation

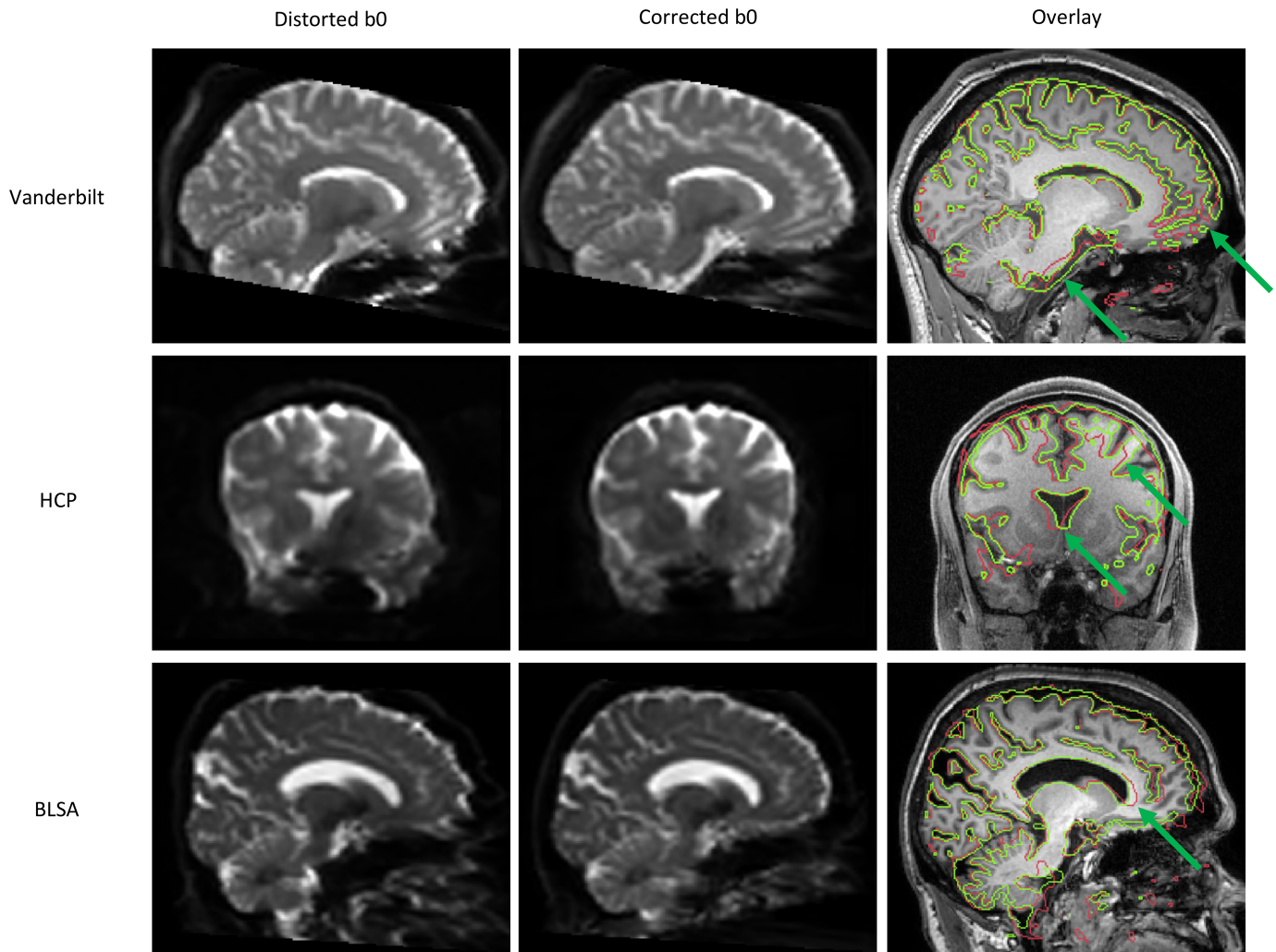


Fig. 6. With-held test set results. Vanderbilt (top), HCP (middle), and BLSA (bottom) datasets, the distorted (left) and undistorted (after applying the proposed pipeline) b0 (right) are shown, and also overlaid on a structurally-undistorted T1 image. This demonstrates qualitatively improved alignment to the subjects' T1 using the proposed pipeline (i.e., synthesized b0 and topup correction). Arrows highlight areas of observable improvement.

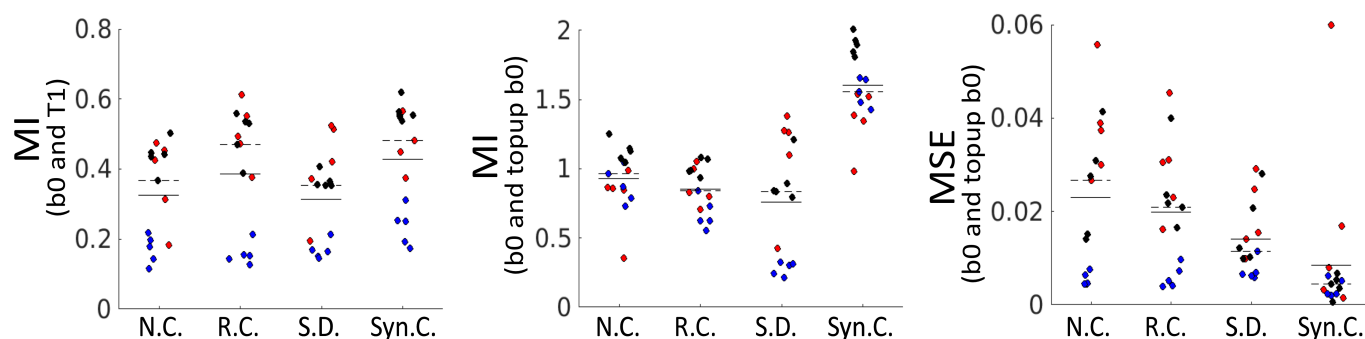


Fig. 7. Validation of geometry and contrast after distortion correction. Top: MI of the non-corrected (N.C.), registration corrected (R.C.), legacy synthetic-distortion (S.D) and proposed synthetic correction (Syn.C.) b0 images with the structural T1 image. A higher value suggests a geometry more similar to the undistorted T1. Middle: MI of the N.C., R.C., S.D., and Syn.C. b0 with state-of-the-art topup distortion correction results. A higher value indicates geometry/contrast more similar to the gold-standard. Bottom: MSE of the N.C., R.C., S.D., and Syn.C., b0 with state-of-the-art topup distortion correction results. A lower value indicates structure and image intensities more similar to the topup results. For both, solid and dashed lines indicate mean and median values, respectively. Each contains 15 datapoints, from 5 HCP subjects (blue), 5 Vanderbilt subjects (black), and 5 BLSA subjects (red).

curves. Training took 2.5 days to complete on a single Nvidia TITAN Xp GPU.

Figure 6 shows results from the withheld test set, including distorted b0 and corrected b0 after application of the proposed distorted correction, for the Vanderbilt, HCP, and BLSA datasets. Note that the corrected b0 in **Figure 6** represents the results of the entire proposed pipeline – synthesizing an undistorted b0, then applying topup to the synthesized images. Thus, we are visualizing *corrected* b0 images and not the *synthesized* images.

The third column of **Figure 6** contains overlays of the outlines of the corrected (green) and distorted (red) b0s. In all cases, it is clear that the corrected b0 is geometrically more similar to the T1 image than uncorrected, indicating significant reductions in distortions. For Vanderbilt data, the most pertinent region of correction is the anterior region of the brain, and mid-brain areas (green arrows). For HCP, left/right distortion is clearly corrected, and is most obvious in the lateral ventricles and superior aspects of the white/gray matter boundary (green arrows). Last, for BLSA, the anterior part of the lateral ventricles is most obviously misaligned with the T1 weighted image (green arrows).

To verify anatomically faithful distortion correction, it is critical to quantify geometric similarity resulting corrected b0 images to the co-registered (and undistorted) T1. **Figure 7** (left) shows the mutual information between a non-corrected b0 (N.C.), registration-corrected b0 (R.C.), and the proposed synthetic-correction (Syn.C.), where a higher value serves as an indicator of a closer match to the structural scan. It is clear that both correction methods significantly improve brain geometry. **Figure 7** (right) quantifies the MSE of each b0 with the state-of-the-art topup-corrected b0. In this case, the synthesized method shows significant improvements in both geometry and contrast (with one outlier). Thus, results are structurally similar to T1, and on par with registration techniques (as assessed by MI to T1) and more closely match the ground truth state of the art topup correction (as assessed by MSE with TOPUP b0).

3.2 Results with External Validation

We apply the proposed synthesis+topup pipeline using data from existing open-sourced diffusion datasets that were not included in training (**Table 1**). **Figure 8** shows that these can correct distortions on datasets that may differ from those the networks were trained on. Specifically, we use the MASSIVE, Age-ility, and Kirby21 datasets, all of which are acquired at varying resolutions, different distortion directions, different brain sizes, and different subject ages. Most areas show significantly improved geometric match to T1's, for example frontal areas, ventricles, and brainstem (green arrows), indicating effective distortion correction. Qualitatively, application of the pipeline results in satisfactory correction despite limited areas where the corrected b0 may have room for improvement (red arrows).

4. Discussion

The Synb0 substantially improves upon the state of the art for distortion correction of DW-MRI data without supplementary acquisitions. Synb0 more accurately identifies anatomical geometry than image-based distortion correction as assessed by mutual information and mean squared error. The improvement is consistent across multiple datasets. Moreover, Synb0 runs in ~2 minutes per scan (specifically, inference, or generation of synthetic images, is ~2 minutes, while application of topup can vary from ~20-40 minutes depending on resolution and topup configuration), versus ~10-15 minutes for image-based registration.

We emphasize that correction without modern/supplementary sequences is not a first choice for study design. However, vast quantities of DW-MRI have been acquired (and are still being acquired) with classic/limited DW-MRI sequences (e.g., legacy studies, older scanners, scanners without advanced DW-MRI license keys, clinically acquired imaging). Hence, it is important to have the best possible alternative processing strategies for these data.

This effort is the second publication to examine deep learning for DW-MRI distortion correction. Mutual information is improved by a mean of 36% over the prior publication and 11% over registration correction (**Figure 4a,b**). On a study by study basis, these are statistically

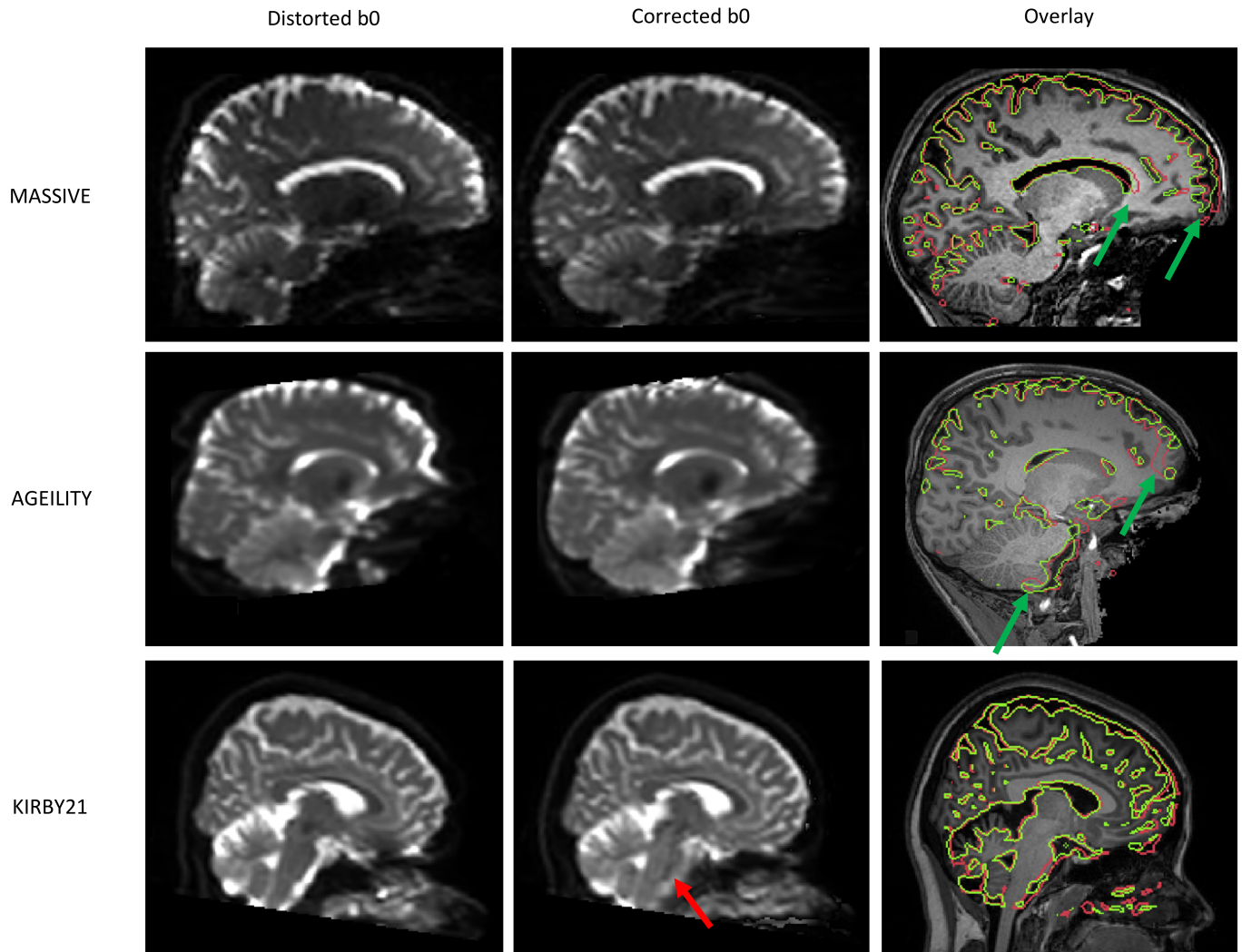


Fig. 8. External dataset validation. External validation of corrected b0's after applying the synthesized b0 distortion correction pipeline with data from open-sourced studies. The distorted and undistorted b0 outlines are shown overlaid on T1 images in green and red, respectively. In all cases, effective distortion correction is visually apparent (green arrows). Note that there was a failure for the cerebral-spinal fluid region near the pons of the brainstem for the KIRBY21 data (red arrows).

significant ($p < 0.001$, paired t-test) across all individual cohorts. Similarly, mean squared error is improved (decreased) by a mean of 40% over the prior publication and 63% over registration correction (**Figure 4c**), with differences in cohorts showing statistical significance ($p < 0.001$, paired t-test).

A Singularity virtual machine image has been made available to enable simple evaluation of the proposed techniques at <https://github.com/MASILab/Synb0-DISCO>. The Singularity requires only a b0 and T1 as inputs, and performs all pre-processing (T1 bias field correction and normalization, registration to MNI), image synthesis or model inference, and topup – returning as output topup field coefficients and all intermediate data. Source code and binaries are available at <https://github.com/MASILab/Synb0-DISCO>. These open source efforts simplify training or transfer learning with larger datasets.

Acknowledgments

This work was conducted in part using the resources of the Advanced Computing Center for Research and Education at Vanderbilt University,

Nashville, TN. This work was supported by the National Institutes of Health under award numbers R01EB017230, and T32EB001628, and in part by ViSE/VICTR VR3029 and the National Center for Research Resources, Grant UL1 RR024975-01, and Department of Defense award number W81XWH-17-2-055. This research was conducted with the support from Intramural Research Program, National Institute on Aging, NIH. The content is solely the responsibility of the authors and does not necessarily represent the official views of the NIH. We gratefully acknowledge the support of NVIDIA Corporation with the donation of the Titan Xp GPU used for this research.

References

1. Wu M, Chang L-C, Walker L, et al. Comparison of EPI distortion correction methods in diffusion tensor MRI using a novel framework. International Conference on Medical Image Computing and Computer-Assisted Intervention; 2008: Springer. p. 321-9.
2. Smith SM, Jenkinson M, Woolrich MW, et al. Advances in functional and structural MR image analysis and implementation as FSL. Neuroimage 2004;23:S208-S19.

3. Graham MS, Drobnyak I, Jenkinson M, Zhang H. Quantitative assessment of the susceptibility artefact and its interaction with motion in diffusion MRI. *PLoS one* 2017;12:e0185647.
4. Sotiropoulos SN, Jbabdi S, Xu J, et al. Advances in diffusion MRI acquisition and processing in the Human Connectome Project. *Neuroimage* 2013;80:125-43.
5. Andersson JL, Skare S, Ashburner J. How to correct susceptibility distortions in spin-echo echo-planar images: application to diffusion tensor imaging. *Neuroimage* 2003;20:870-88.
6. Irfanoglu MO, Nayak A, Jenkins J, Pierpaoli C. TORTOISE v3: Improvements and New Features of the NIH Diffusion MRI Processing Pipeline. Proceedings of the 25th Annual Meeting of ISMRM Presented at the International Society for Magnetic Resonance in Medicine; 2017: ISMRM Hawaii, USA.
7. Andersson JL, Sotiropoulos SN. An integrated approach to correction for off-resonance effects and subject movement in diffusion MR imaging. *Neuroimage* 2016;125:1063-78.
8. Irfanoglu MO, Modi P, Nayak A, Hutchinson EB, Sarlls J, Pierpaoli C. DR-BUDDI (Diffeomorphic Registration for Blip-Up blip-Down Diffusion Imaging) method for correcting echo planar imaging distortions. *NeuroImage* 2015;106:284-99.
9. Irfanoglu MO, Sarlls J, Nayak A, Pierpaoli C. Evaluating corrections for Eddy-currents and other EPI distortions in diffusion MRI: methodology and a dataset for benchmarking. *Magnetic resonance in medicine* 2019;81:2774-87.
10. Brun L, Pron A, Sein J, Deruelle C, Coulon O. Diffusion MRI: Assessment of the Impact of Acquisition and Preprocessing Methods Using the BrainVISA-Diffuse Toolbox. *Frontiers in neuroscience* 2019;13:536.
11. Bastiani M, Cottaar M, Fitzgibbon SP, et al. Automated quality control for within and between studies diffusion MRI data using a non-parametric framework for movement and distortion correction. *NeuroImage* 2019;184:801-12.
12. Usman M, Kakkar L, Kirkham A, Arridge S, Atkinson D. Model-based reconstruction framework for correction of signal pile-up and geometric distortions in prostate diffusion MRI. *Magnetic resonance in medicine* 2019;81:1979-92.
13. Snoussi H, Caruyer E, Cohen-Adad J, et al. Geometric evaluation of distortion correction methods in diffusion MRI of the spinal cord. *IEEE International Symposium on Biomedical Imaging (ISBI)*; 2019.
14. Schilling KG, Blaber J, Huo Y, et al. Synthesized b0 for diffusion distortion correction (Synb0-DisCo). *Magn Reson Imaging* 2019;64:62-70.
15. Froeling M, Tax CMW, Vos SB, Luijten PR, Leemans A. "MASSIVE" brain dataset: Multiple acquisitions for standardization of structural imaging validation and evaluation. *Magnetic resonance in medicine : official journal of the Society of Magnetic Resonance in Medicine / Society of Magnetic Resonance in Medicine* 2017;77:1797-809.
16. Landman BA, Huang AJ, Gifford A, et al. Multi-parametric neuroimaging reproducibility: a 3-T resource study. *NeuroImage* 2011;54:2854-66.
17. Karayanidis F, Keuken MC, Wong A, et al. The Age-ility Project (Phase 1): Structural and functional imaging and electrophysiological data repository. *NeuroImage* 2016;124:1137-42.
18. Fischl B. *FreeSurfer*. *Neuroimage* 2012;62:774-81.
19. Avants BB, Tustison N, Song G. Advanced normalization tools (ANTS). *Insight j* 2009;2:1-35.
20. Ronneberger O, Fischer P, Brox T. U-net: Convolutional networks for biomedical image segmentation. *International Conference on Medical image computing and computer-assisted intervention*; 2015: Springer. p. 234-41.
21. Çiçek Ö, Abdulkadir A, Lienkamp SS, Brox T, Ronneberger O. 3D U-Net: learning dense volumetric segmentation from sparse annotation. *International conference on medical image computing and computer-assisted intervention*; 2016: Springer. p. 424-32.
22. Paszke A, Gross S, Chintala S, et al. *Automatic differentiation in pytorch*. 2017.
23. Gorgolewski KJ, Alfaro-Almagro F, Auer T, et al. BIDS apps: Improving ease of use, accessibility, and reproducibility of neuroimaging data analysis methods. *PLoS computational biology* 2017;13:e1005209.
24. Liu C-F, Padhy S, Ramachandran S, et al. Using Deep Siamese Neural Networks for Detection of Brain Asymmetries Associated with Alzheimer's Disease and Mild Cognitive Impairment. *Magn Reson Imaging* 2019.
25. Nath V, Parvathaneni P, Hansen CB, et al. Inter-Scanner Harmonization of High Angular Resolution DW-MRI using Null Space Deep Learning. *International Conference on Medical Image Computing and Computer-Assisted Intervention*; 2018: Springer. p. 193-201.
26. Bhushan C, Haldar JP, Joshi AA, Leahy RM. Correcting susceptibility-induced distortion in diffusion-weighted MRI using constrained nonrigid registration. *Proceedings of the 2012 Asia Pacific Signal and Information Processing Association Annual Summit and Conference*; 2012: IEEE. p. 1-9.
27. Shattuck DW, Leahy RM. *BrainSuite: an automated cortical surface identification tool*. *Medical image analysis* 2002;6:129-42.

